https://doi.org/10.5194/egusphere-2023-2321
Preprint. Discussion started: 21 December 2023

Exploring the use of Sentinel-1 to monitor spatial and temporal evolution of permafrost in the Swiss Alps

Kristina Reinders[1], Govert Verhoeven[2], Luca Sartorelli[3], Ramon Hanssen[1], and Andrea Manconi[4,5]

[1]Delft University of Technology, The Netherlands
[2]University of Bern, Switzerland
[3]SkyGeo, The Netherlands
[4]WSL Institute for Snow and Avalanche Research SLF, Switzerland
[5]Climate Change, Extremes and Natural Hazards in Alpine Regions Research Centre CERC

Correspondence: Kristina Reinders (k.j.reinders@tudelft.nl)

Abstract.

In this work, we assess the performance of Persistent Scatterer Interferometry (PSI) based on Sentinel-1 data in the Swiss Alps, focusing on the analysis of surface displacement in areas located in permafrost. To this end, we exploit a PSI dataset over Canton Wallis and the recently published permafrost and ground ice map of Switzerland (PGIM). First we evaluate the sensitivity to radar detection of the terrain, given a particular slope distribution and given satellite orbital geometries. We find that 92% of the areas currently labeled as permafrost satisfy the geometric visibility criteria, which is a necessary but not sufficient condition for detection of ground movement by satellite radar. Second, we analyse the PSI surface velocity and displacement time series observed in Canton Wallis in the period 2015 to 2022. We find that the displacements rates appear to be correlated with the occurrence of permafrost and that there is a significant difference in displacement rates between ice-poor and ice-rich permafrost compared to no-permafrost zones. However, the difference between the surface velocities retrieved in ice-poor permafrost and no-permafrost zones are small and additional information would be needed to discriminate ice-poor permafrost zones.

1 Introduction

In alpine regions climate change is occurring at a faster pace than elsewhere in the world. (IPCC, 2018; Goodfellow and Boelhouwers, 2013). In the Austrian and Swiss Alps temperature has increased with 2 °C between the end of the nineteenth and the beginning of the twenty-first century (Auer et al., 2007) and it is predicted that in the Swiss Alps the annual average temperature will rise by an additional 2.1 to 3.7 °C by the middle of the 21st century, if global greenhouse gas emissions continue to rise at the current rate (CH2018, 2018). Besides the rise in temperature, the number of days with fresh snowfall will likely decrease (Meteoschweiz). These processes affect in particular the mountain cryosphere. Measurements show that since the year 2000 ground surface temperatures raised (Etzelmüller et al., 2020) and snow cover, glaciers and permafrost declined and it is expected that this decline will continue in almost all regions throughout the 21st century (Hock et al., 2019). Currently, permafrost in the Alps occurs at elevations above 2500 m, but predictions show that the permafrost boundary will rise in the 21st

https://doi.org/10.5194/egusphere-2023-2321
Preprint. Discussion started: 21 December 2023

century (Magnin et al., 2017). Permafrost consists of an active layer at the surface that freezes and thaws each year, underlain by perennially frozen ground.The active layer thickness (ALT) in 2022 was between around 2 and 13 m in the boreholes from the PERMOS Network (PERMOS), with an average of around 5 meters. Thickening of the active layer, warming of the permafrost body itself and the disappearance of the permafrost (Ravanel et al., 2017) is called permafrost degradation. The Intergovernmental Panel on Climate Change (IPCC) refers to permafrost degradation as a naturally or artificially caused decrease in the thickness and/or areal extent of permafrost. Due to this temperature rise the soil strength decreases because in general frozen soil has higher strength. This can lead to deformations and reduced bearing capacity of the ground.

Permafrost in Switzerland covers about 3.5% of the national territory (SLF). Fig. 1 shows the permafrost zones in the Swiss Alps according to the most recent version of the permafrost map of the Swiss Institute for Snow and Avalanche Research (PGIM).It shows the permafrost distribution in the Swiss Alps and has a variable uncertainty (Kenner et al., 2019; SLF). The area of canton Wallis is highlighted because this is the study area of our research.

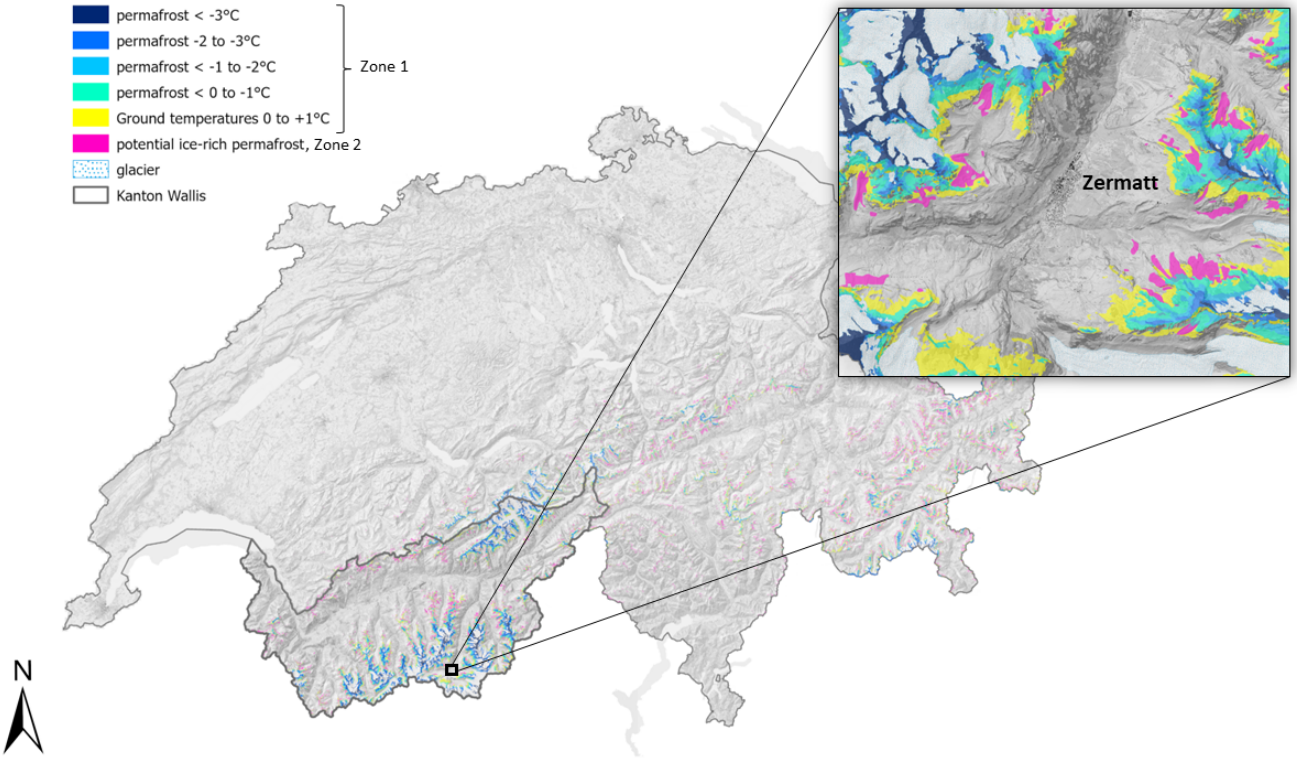

Figure 1. Permafrost and ground ice map (PGIM), canton Wallis highlighted.

The correlation between surface deformations and alpine permafrost degradation has been difficult to prove in the past. However, more and more evidence is becoming available that changing alpine permafrost conditions may alter the frequency and magnitude of mass movements, may result in an increase in slope instabilities, rockfalls and debris flow activity or even a

https://doi.org/10.5194/egusphere-2023-2321
Preprint. Discussion started: 21 December 2023

destabilisation of rock glaciers (Baral et al., 2023; Jones et al., 2023; Noetzli and Phillips, 2019; Patton et al., 2019; Krautblatter et al., 2013; Gruber and Haeberli, 2007; Noetzli et al., 2007). Many mountain (infra)structures such as cable-cars, railways, avalanche barriers, communication and electricity lines, as well as mountain cabins, that are located in high alpine areas, can be affected by changing permafrost conditions. As these infrastructures are important for tourism, communication, power supply, and other human activities, it is essential to accurately map permafrost in order to assess the vulnerability of these areas and estimate the potential natural hazards.

Currently, the most common method to assess permafrost stability are temperature measurements in boreholes. For the Swiss Alps, a permafrost monitoring network (PERMOS) exists since the 1990s, which contains 14 borehole sites (PERMOS). However drilling boreholes and monitoring temperatures in this high alpine environment can be difficult, labor-intensive and expensive (Noetzli et al., 2021). Also, the boreholes are often distributed unevenly from a geographical perspective and biased toward more accessible locations or pre-existing research sites (Hock et al., 2019).

Since more than 30 years, Interferometric Synthetic Aperture Radar (InSAR) has proven to be a valid alternative to monitor ground displacements (Hanssen, 2001). This remote sensing technique can measure displacements of the ground based on the phase difference of two SAR images, acquired over the same area at different times. InSAR has been extensively used for monitoring subsidence, landslides, buildings and infrastructure, and also successfully used in permafrost areas (Wang et al., 2023; Li et al., 2021; Liu et al., 2022; Rouyet et al., 2019; Daout et al., 2017; Abe et al., 2020; Liu et al., 2015). An overview of the available literature and the limitations and potential of this technique for these applications is given in (Macchiarulo et al., 2022; Reinders et al., 2022; Barboux et al., 2013). Freely available SAR data from satellite missions such as the ESA Copernicus Sentinel-1 mission have made InSAR technology even more accesible. This data provide new opportunities for wide-area ground motion detection and monitoring. At regional and national scale publicly available Persistent Scatterer Interferometry (PSI) maps are being produced (Crosetto et al., 2020), see, e.g., (NCG; Kanton Wallis, a; WSP and Skygeo; NGU et al.; BGR; UNIFI). Also the European Ground Motion Service (EGMS) provides ground deformation over most of Europe, based on Sentinel-1 SAR data (EGMS). While all these maps are 'application-agnostic', indicating that they are not optimized for a particular application or location, they provide valuable insights. Successful ground deformation estimation using satellite InSAR minimally requires (i) a location-of-interest that is sensitive to deformation by the radar, (ii) coherent phase-interpretable scatterers, and (iii) sufficient radar acquisitions to produce displacement time series.

The objective of this study is to assess the possibilities and limitations of Sentinel-1 PSI data to evaluate and validate conventional alpine permafrost maps focusing on the Swiss Alps. Permafrost maps show the geographic zones where permafrost is observed or expected. First we investigate how much of the permafrost zones are sensitive to radar detection with Sentinel-1. Second, we examine whether ground deformation trends estimated from the Sentinel-1 based available regional Persistent Scatterer Interferometry (PSI) map of Canton Wallis in Switzerland can be correlated with the known permafrost zones, as mapped in the permafrost and ground ice map (PGIM) of the Swiss Institute for Snow and Avalanche Research (Kenner et al., 2019; SLF). Finally we investigate if this available PSI map of Canton Wallis can be used as a tool to validate and update the current PGIM permafrost map of Switzerland.

https://doi.org/10.5194/egusphere-2023-2321
Preprint. Discussion started: 21 December 2023

2 Data and Methods

For this study, we use the orbits of Sentinel-1 over entire Switzerland, i.e. descending tracks 136, 66, 168, and ascending tracks 88 and 15 (The European Space Agency, a)(See Fig. **??**) and the Copernicus 30 m resolution Digital Elevation Model (DEM) (The European Space Agency, b) for producing the sensitivity map. Next, we use the pre-existing Persistent Scatterer Interferometry (PSI) result which is available over the canton Wallis in Switzerland (Kanton Wallis, a) and the most recent version of the permafrost and ground ice map (PGIM) from the Swiss Institute for Snow and Avalanche Research (Kenner et al., 2019; SLF) to examine ground deformation trends in permafrost. Finally, for one location within Canton Wallis, Alpage de Mille, displacement data from repeated GNSS and total station surveys (PERMOS) are compared to the PSI map.

2.1 Nationwide Sentinel-1 sensitivity map

The InSAR displacement detection potential and the sensitivity to radar detection of the areas of interest can be evaluated before actual satellite data processing. Combining slopes and aspects from the DEM with the incidence angles and the orientation of the zero-Doppler plane towards the satellite, foreshortening, layover, and shadow regions can be determined. Moreover, assuming downslope motion, the sensitivity of detection can be computed from the projection of the displacement vector onto the line-of-sight vector. (Notti et al., 2014; Chang et al., 2018; van Natijne et al., 2022a; Brouwer and Hanssen, 2023a). The R-index, with $R \in [-1, 1]$, (Notti et al., 2014) is a metric that allows combining the visibility of the satellite—i.e., $-1 < R \leq 0$ indicates no visibility—with the sensitivity for detecting down-slope motion, where greater values for R refer to higher sensitivity. Table 1 gives an indication of the sensitivity to downslope motion.

Table 1. R-index interpretation modified from Notti et al. (2014).

R-index	sensitivity
$-1 \leq R$-index ≤ 0	No visibility towards satellite due to layover, shadow, or foreshortening
$0 < R$-index ≤ 0.3	very little sensitivity to downslope motion
$0.3 < R$-index ≤ 0.5	moderate sensitivity to downslope motion
$0.5 < R$-index ≤ 1	sufficient sensitivity to downslope motion

Note that the condition of a positive R value is necessary but not sufficient, as the occurrence of coherent objects is also highly dependent on surface conditions.

To compute the R-index, we pre-process the Sentinel-1 data downloaded from the Copernicus Open Access Hub (The European Space Agency, a) per orbital geometry using the ESA SNAP Sentinel-1 toolbox and the Copernicus DEM (The European Space Agency, b). We use data for descending tracks 136, 66, 168, and ascending tracks 88 and 15, see Fig. 2 for a top-view of the tracks. Table. 2 lists the used Sentinel tracks and the relevant geometry parameters for our Area of Interest (AoI), i.e. Switzerland. The azimuth of the zero-Doppler plane, α_d, is defined at a geographic location, in the direction towards

https://doi.org/10.5194/egusphere-2023-2321
Preprint. Discussion started: 21 December 2023

Table 2. Sentinel-1 data covering Switzerland, see Fig. **??**. ZDP is the zero-Doppler plane.

Track		Incidence Angle, θ within the AoI [deg]	Azimuth ZDP, α_d [deg]
88	ascending	32.4 to 45.9	255.71
15	ascending	37.0 to 44.6	255.87
139	descending	37.0 to 40.8	104.50
66	descending	37.0 to 45.9	104.69
168	descending	39.5 to 45.9	104.49

the satellite. It is based on the heading of the satellite, correcting for the range-dependent meridian convergence (Brouwer and Hanssen, 2023a)

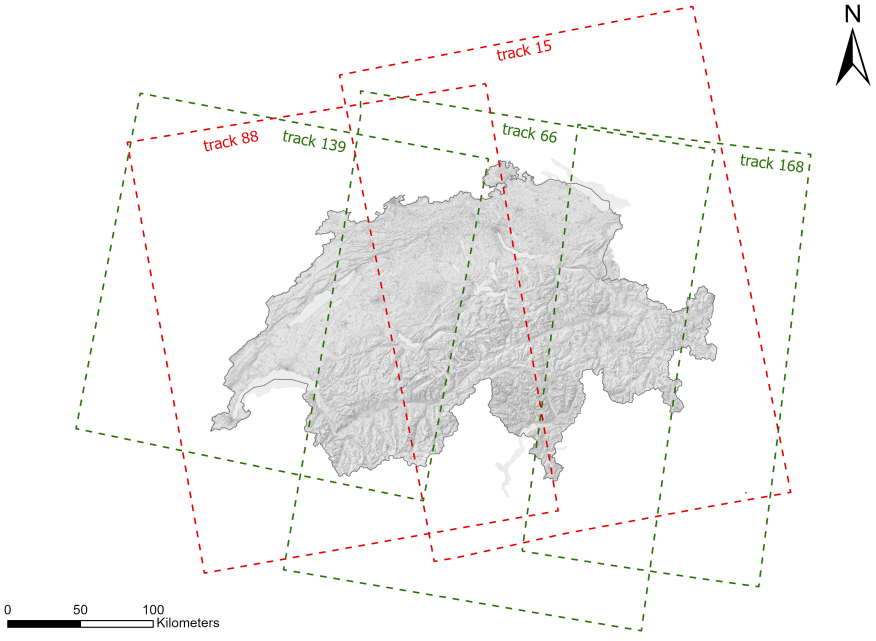

Figure 2. Topview of the ascending (red) and descending (green) Sentinel-1 images over Switzerland.

We import the results into a geographical information system, and create geotiff files containing the shadow and layover mask, the local slope β and aspect α angles, and the incidence angle θ, following Del Soldato et al. (2021).

The R-index for geographic location (ϕ, λ) can be expressed as:

$$R(\phi,\lambda) = \begin{cases} \sin\big(\theta - \beta\cos(\alpha_d - \alpha)\big) & \text{if } S_h = 1 \wedge L = 1 \\ 0 & \text{otherwise,} \end{cases} \tag{1}$$

https://doi.org/10.5194/egusphere-2023-2321
Preprint. Discussion started: 21 December 2023

where $S_h \in \{0,1\}$ and $L \in \{0,1\}$ are binary indicators for the absence (0) or occurrence (1) of shadow and the layover, respectively.

We create one map with the R-index of the Swiss Alps for ascending tracks and one map for descending tracks. In the overlap area, we select the track in the far range, i.e., greater incidence angle because the extent of layover areas is much greater than shadow areas in our analysis.

Finally we repeat the computation with the global sensitivity index for landslide deformation Google Earth Engine tool of van Natijne et al. (2022b, a) and obtain similar results.

2.2 Regional PSI map of Canton Wallis

Canton Wallis is an administrative subdivisions in the southern part of Switzerland. In Wallis the highest mountains of Switzerland are located and the elevation from the lowest valley to the highest top is between 370 m and 4630 m above sea level. The five villages with the the largest amount of inhabitants are located between 400 and 700 m above sea level and are situated in the Rhone valley. In the side valleys, the elevation of the villages reaches 1900 m. Wallis is one of the cantons with the most permafrost area in Switzerland. Due to its geographical location and climatic conditions, it is particularly exposed to natural hazards, such as floods, inundations, avalanches, debris flows, rock falls, landslides and also forest fires and droughts. Interactive hazard maps are available for the different hazards and over 200 unstable areas are actively monitored (Kanton Wallis, b). Since 2003, the canton has been equipped with a remote monitoring network of automated measurement stations, measuring deformation and hydrometeorological data. All monitoring data is integrated in Guardaval, a system for the automatic and continuous retrieval of these measurements, their storage, and their publication via a webviewer.

This Guardaval platform contains information about past and known landslides and rockfall areas, precipitation, and temperature. It also contains a Persistent Scatterer Interferometry (PSI) map of Canton Wallis. This PSI result is applied to detect deformation, but it is not computed specific for the purpose of permafrost zonation evaluation. This data is available through an online webviewer and accessible to selected stakeholders and scientists (Kanton Wallis, a). The map contains more than 4.5 million Persistent Scatterers (PS) from Sentinel-1 descending track 66, and more than 3.8 million PS from ascending track 88, including time series with line-of-sight displacements covering the period 2015 to 2022. Due to snow cover, and associated loss of coherence, winter images were removed. The time period with the presence of snow varies per location and altitude. In our area of interest, only data between early June and early November are available on the webviewer, with a 6 to 12 day interval. Fig. 3a shows the number of acquisitions within this seasonal window for both orbits per year for our area of interest, indicating that the number of acquisitions is significant. Fig. 3b shows the number of PS per elevation interval, indicating that the majority of coherent PS are situated at elevations well above the urban areas. The geolocation precision of these points is 20 m (Kanton Wallis, a). In our analyses, we use the linear line-of-sight displacement rates of all PS of Sentinel-1.

2.3 PGIM Permafrost maps

Several alpine permafrost maps were published the last decades. In 2005, the Federal Office for the Environment published an map, showing the potential permafrost distribution in Switzerland (Bundesamt für Umwelt, 2005). Later, the permafrost and

https://doi.org/10.5194/egusphere-2023-2321
Preprint. Discussion started: 21 December 2023

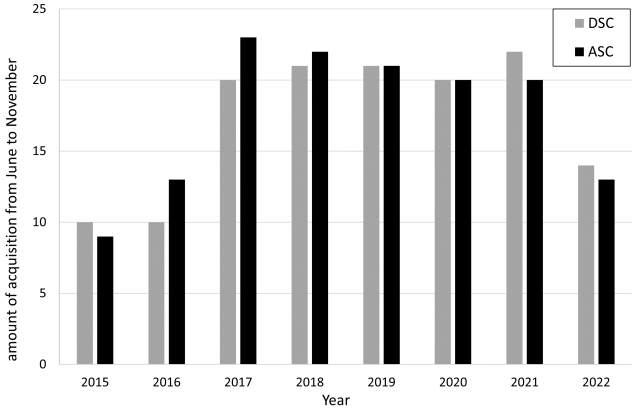

(a) Number of acquisitions within the seasonal window in our area of interest.

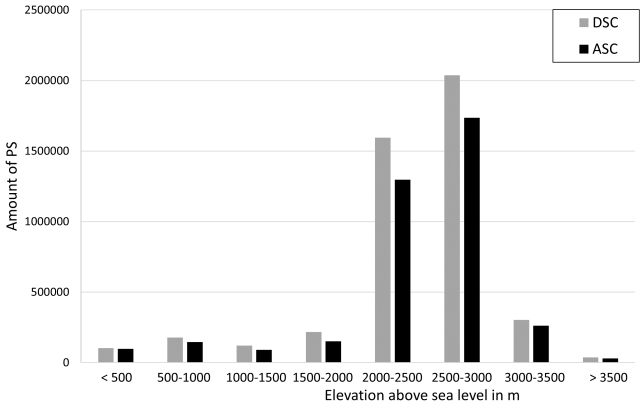

(b) Number of coherent point scatterers per elevation interval.

Figure 3. Number of Sentinel acquisitions per year and number of coherent point scatterers per elevation for the PSI map of Canton Wallis.

ground ice map, called PGIM, was developed by the Swiss Institute for Snow and Avalanche Research (Kenner et al., 2019; SLF), see Fig. 1. In this map the total permafrost area is around 1400 km^2 (Kenner et al., 2019).

This PGIM is an indication map for the occurrence of permafrost (SLF). It is based on models that include elevation, potential incoming solar radiation, and the deposition zones of alpine mass wasting processes (Kenner et al., 2019). Also data from the current permafrost network (PERMOS) is included, which observes permafrost conditions at 27 sites located between 2200 and 3500 m in the Swiss Alps. It distinguishes ice-poor zones (zone-1) and ice-rich zones (zone-2). Zone-1 consist of all areas with modelled negative ground temperatures and a buffer area with ground temperatures ranging between 0 and 1 °C. In Fig. 1 these are the permafrost zones from < -3 °C to $+1$ °C. Zone-2 is generally located at lower altitudes and consists of rock glaciers or ice-rich talus slopes. A rock glacier is a lobate or tongue-shaped landform consisting of rock debris and either an ice core or an ice-cemented matrix, creeping down mountain slopes (Giardino et al., 2011) with a velocity of centimeters to meters per year (Noetzli and Pellet, 2023). This movement is not necessarily constant and can show a seasonal pattern with faster or slower displacement (Delaloye et al., 2010) or even phases without movement (Brencher et al., 2020). There is a large uncertainty in the mapping of the ice-rich permafros (Kenner et al., 2019).

According to RGIK (2021) functional rock glaciers are geomorphological indicators of permafrost occurrence and can be used to approximate the regional lower limit of the mountain permafrost belt. In Fig. 1 this is the ice-rich permafrost zone. In the PGIM all areas steeper than 30° were removed in zone-2 because they barely contain ice-rich permafrost (Kenner et al., 2019). Also all glaciers were excluded in the PGIM and therefore they are also excluded in our analyses.

https://doi.org/10.5194/egusphere-2023-2321
Preprint. Discussion started: 21 December 2023

3 Results

In the following sections, we first present a map showing the sensitivity to radar detection of permafrost zones in the Swiss alps. Next we combine the PSI map of Canton Wallis with the PGIM to identify differences in deformations in permafrost and no permafrost zones and finally we compare the PSI data with geodetic displacement data from the Permos network for one location in the Swiss Alps.

3.1 Sensitivity to radar detection of permafrost zones

To assess which permafrost zones in the Swiss Alps are sensitive to detection with Sentinel-1, we combine the PGIM with the R-index map of Switzerland. This results in a map presenting the sensitivity to radar detection of the permafrost zones. Fig. 4 indicates areas with an R-index between 0.5 and 1, which refers to sufficient sensitivity to displacements, for both the ascending and descending orbits for the permafrost zones in Switzerland, see Table **??**. We find that 68% of the permafrost

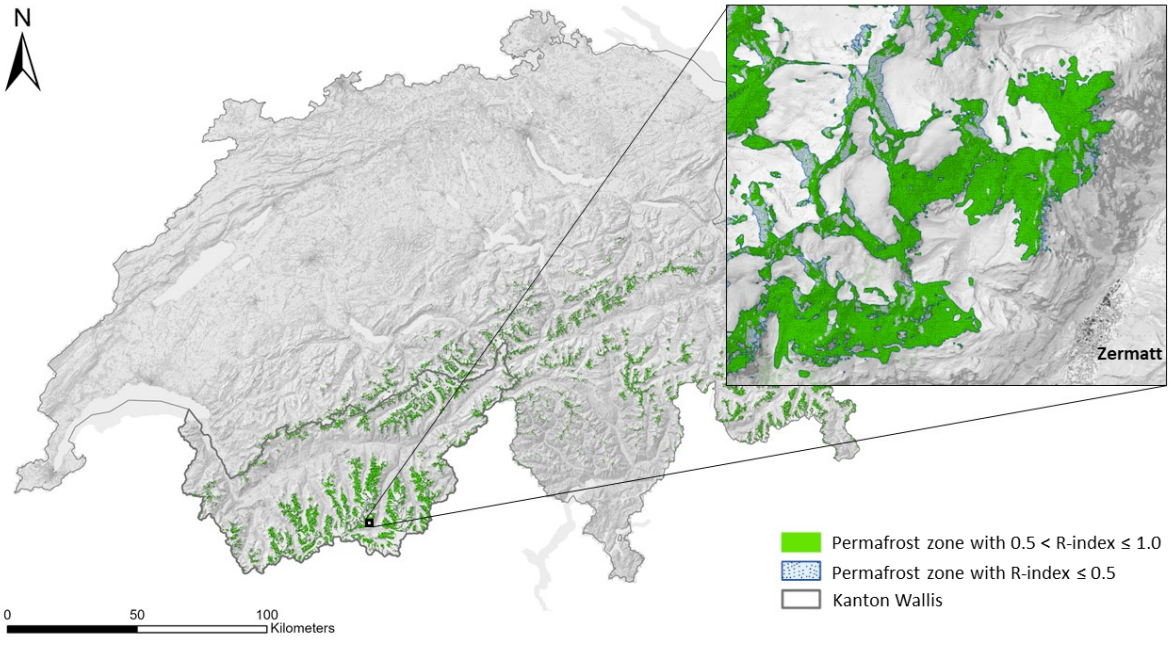

Figure 4. Permafrost zones according to the PGIM including the sensitivity. Permafrost areas with R-index values between 0.5 and 1 in green, permafrost areas with smaller R-index in blue. Ascending and descending orbits are combined.

zones have sufficient sensitivity to radar detection (i.e., R-index > 0.5) from the descending track and 63% from the ascending track, see Table 3. 92% of the currently mapped permafrost zones in the PGIM have sufficient sensitivity to radar detection for at least one orbital geometry and ∼39% of the PGIM permafrost area have sufficient sensitivity to radar detection for both ascending and descending orbits.

https://doi.org/10.5194/egusphere-2023-2321
Preprint. Discussion started: 21 December 2023

Table 3. R-index of the permafrost zones in Switzerland with Sentinel-1

R-index value	Areal coverage of labeled permafrost zones from descending orbit [%]	Areal coverage of labeled permafrost zones from ascending orbit [%]	Combined areal coverage (descending and ascending) [%]
shadow/layover (R-index=0)	15	16	
0 < R-index $\leqq$ 0.3	4	5	
0.3 < R-index $\leqq$ 0.5	14	16	
0.5 < R-index $\leqq$ 1	68	63	92

Table 4. Data characteristics of PS map of Wallis

	#PS	#PS per 100×100 m	mean velocity [mm/y]	st.dev velocity [mm/y]	median velocity [mm/y]
Descending track					
No-Permafrost	3 250 000	7	−0.89	3.69	−0.14
Ice-poor permafrost (zone-1)	840 000	13	−1.16	4.29	−0.12
Ice-rich permafrost (zone-2)	500 000	30	−2.42	8.10	−0.45
Ascending track					
No-Permafrost	2 650 000	6	−0.49	2.96	0.03
Ice-poor permafrost (zone-1)	700 000	11	−0.60	3.49	0.14
Ice-rich permafrost (zone-2)	475 000	28	−1.52	4.78	−0.16

3.2 Comparison permafrost zones with deformation data from regional PSI map of Canton Wallis

We combine the reference permafrost map, i.e. PGIM, with the the Persistent Scatterer Interferometry (PSI) map of canton Wallis (Kanton Wallis, a). The PGIM distinguishes three zones: no-permafrost, ice-poor permafrost (i.e., zone-1), and ice-rich permafrost (i.e., zone-2). We identify all PS of the descending and ascending orbits in these three zones and extract the average linear velocities of each PS. Then we calculate the mean, median, and standard deviation of these velocities for all PS in each of the three zones. Table 4 shows the results.

In order to identify differences among the mean velocity of the three zones, the analysis of variance (ANOVA) along with Tukey's range test are used (Tukey, 1949). For the analyses a 95% family-wise confidence level was selected. As null-hypothesis we assume equal means between the three zones, i.e., no difference in displacement rates between no-permafrost, ice-rich permafrost, and ice-poor permafrost.

The outcome of the analyses show that the P-values for both the descending and ascending orbit are less than $2e^{-16}$, indicating that the differences in displacement rates between the three zones are statistically significant for both the ascending

https://doi.org/10.5194/egusphere-2023-2321
Preprint. Discussion started: 21 December 2023

Table 5. Results of the multiple pairwise-comparison of the displacements/year (mm/year) in the three zones for the ascending orbit

	Difference in mean	lower bound of 95% confidence interval	upper bound of 95% confidence interval	P-value
Ice-poor (zone-1) versus no-permafrost	−0.11	−0.12	−0.10	$2e^{-16}$
Ice-rich (zone-2) versus no-permafrost	−1.04	−1.05	−1.03	$2e^{-16}$
Ice-rich (zone-2) versus Ice-poor Permafrost (zone-1)	−0.93	−0.94	−0.91	$2e^{-16}$

Table 6. Example of ANOVA with random sampling of PS for the ascending orbit

	Amount of PS	mean velocity [mm/y]	stand.dev. velocity [mm/y]
Ascending track			
Random Sample 1	500 000	−0.63	3.34
Random Sample 2	500 000	−0.63	3.35
Random Sample 3	500 000	−0.63	3.34
P-value : 0.807			

and the descending track. Ice-rich permafrost zones show a mean velocity of two to three times as high as the mean velocity in no-permafrost zones. The mean velocity in ice-rich permafrost appears to be 2 to 2.5 times as high as in ice-poor permafrost. The mean velocity in ice-poor permafrost is 1.2 to 1.3 times as high as in no-permafrost zones. Fig. 5 shows the results of this test. Outliers were removed to improve the visibility and clarity of the figure. Also, our analyses of multiple pairwise-comparison, i.e. (i) no-permafrost versus ice-poor permafrost (zone-1), (ii) no-permafrost versus ice-rich permafrost (zone-2), and (iii) ice-poor permafrost versus ice-rich permafrost, shows that there is a difference between the means with a confidence level of 95%. Table 5 shows the difference in the means and the lower and the upper end point of the 95% confidence interval. Therefore we reject the null hypothesis and we prove that there is a significant difference between the 3 groups. Ice-rich permafrost zones (zone-2) have a greater velocity than ice-poor permafrost (zone-1) and no-permafrost zones. The results suggest that in Wallis no-permafrost zones have smaller average displacement rates than permafrost zones. This is in line with Penna et al. (2022), who showed that, in general, large unstable rock-slopes with no-permafrost show lower displacement rates than those with permafrost.

To check if the difference in means between the three zones is indeed statistically significant we randomly sample three sets of 100.000 points, with unique samples in each set, and repeat the analysis of variance. This analysis is performed ten times. Then we conduct the same analysis with three sets of 500.000 points. The result show that the P-value for the sets of 100.000 points and the sets of 500.000 points is greater than 0.05, which implies that the difference in means is statistically insignificant. Thus, by random sampling the means of each set are almost the equal. Table 6 shows the results of one calculation with three samples of 500.000 points.

https://doi.org/10.5194/egusphere-2023-2321
Preprint. Discussion started: 21 December 2023

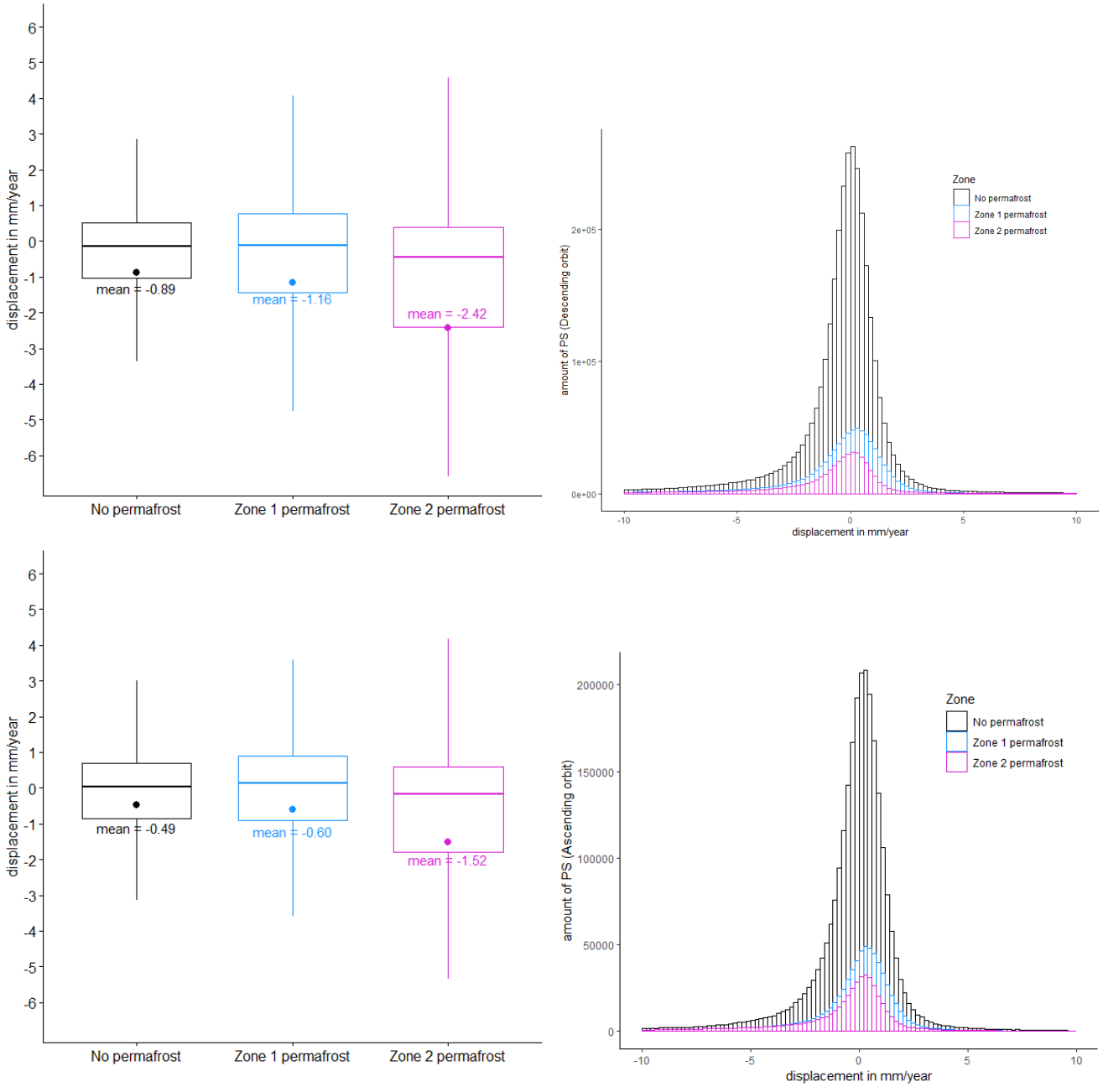

Figure 5. Boxplot with displacements without the outliers (left), histogram of displacements (right). Descending track (top), Ascending track (bottom).

https://doi.org/10.5194/egusphere-2023-2321
Preprint. Discussion started: 21 December 2023

Table 7. ANOVA with PS in no-permafrost zones >2500 m for the ascending orbit

	Amount of PS	mean velocity [mm/y]	stand.dev. velocity [mm/y]
Descending track			
No-permafrost >2500 m	2 662 375	−0.48	2.96
Ice-poor permafrost (zone-1)	700 000	−0.59	3.49
Ice-rich permafrost (zone-2)	475 000	−1.52	4.78
P-value : $<2e^{-16}$			

Table 8. Effect size according to Cohen's d

	DSC	ASC
Ice-poor permafrost (zone-1) – No-permafrost	0.071	0.035
Ice-rich permafrost (zone-2) – No-permafrost	0.374	0.315
Ice-rich permafrost (zone-2) – Ice-poor permafrost (zone-1)	0.259	0.239

Next, to prove that the significant difference between no-permafrost, ice-poor, and ice-rich permafrost is not merely due to elevation, we create a data set with only PS above 2500 m altitude in the no-permafrost zones and include the PS of permafrost zones 1 and 2, which are already located at high elevation, see the elevation distribution in Fig. 3. With this data set we also perform an analysis of variance. The result shows that the P-value is less than $2e^{-16}$, which implies that the difference in means is statistically significant at the 95% confidence level. This proves that we are not correlating height with permafrost, see Table 7.

We therefore conclude that the difference in means between the three zones is indeed significant. However, as the data set is very large, the Tukey's range test has large power, which means that the results will be statistically significant in most cases. Therefore we looked at the practical significance as well by taking into account the effect size. Effect sizes helps decide whether the difference found is meaningful or not. One method to evaluate the effect size is with Cohen's d. This value is based on the difference between two means and divided by the data's standard deviation. It reveals how many standard deviations lie between the two means. According to Cohen (Cohen, 1988), an effect size of 0.2 is considered small, an effect size of 0.5 medium, and an effect size of 0.8 is large. However, these effect size labels are subjective and need to be interpreted in the context of the research (Cohen, 1988). There is no unambiguous method to determine whether a value for the effect size is of practical importance. Observed effect sizes must be judged in context and even small effects might be of practical importance. An effect size of 0.01 can be considered as very small, 0.2 as small, 0.5 as medium, 0.8 as large and beyond 1.2 very large to huge (Sawilowsky, 2009). Table 8 shows Cohen's d for the three zones for ascending and descending orbits.

Our results show that according to Cohen (1988) and Sawilowsky (2009) there is a small to moderate effect between permafrost zone-2 and the no-permafrost zone and between permafrost zone-1 and permafrost zone-2. The results also shows that there is an extremely small effect between permafrost zone-1 and no-permafrost.

https://doi.org/10.5194/egusphere-2023-2321
Preprint. Discussion started: 21 December 2023

3.3 Comparison PSI map with Permos Network measurements

Finally we use geodetic displacement data from the Permos network (PERMOS), acquired by repeated GNSS and total station surveys between 2016 and 2022, and compare it to the PSI map. Fig. 6 shows the Alpage de Mille site, mapped in purple as permafrost zone-2. The right side of the figure shows the velocity from the terrestrial geodetic data, projected onto the line-of-sight to the ascending Sentinel orbit. The left figure show the deformation estimated from the PSI maps, in ascending viewing geometry. The PSI maps corroborate the terrestrial results in terms of the location and extent of displacements. Yet,

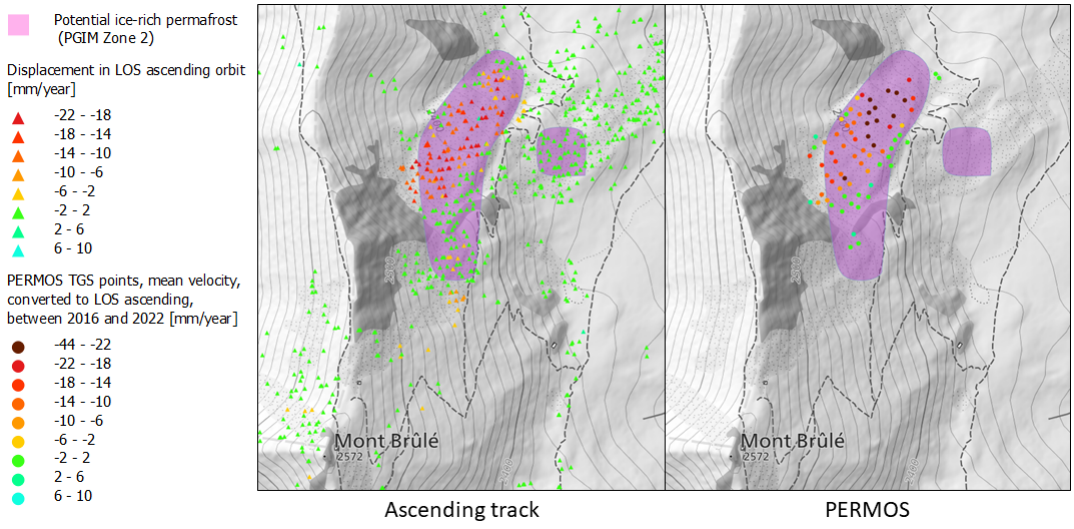

Figure 6. Local comparison between velocity derived from terrestrial observations and projected onto the line-of-sight to the ascending orbit and displacement of ascending orbit from the PSI Map.

the PSI map has a wider coverage in comparison to the existing geodetic benchmarks. This includes estimates for the purple patch to the east of the main Zone-2. The absence of significant displacements at this patch could be a reason to reconsider the attribution of zone-2 permafrost to this region, i.e., this location may not contain ice-rich permafrost.

This example demonstrates the value of the wider coverage of the existing PSI results, e.g. for hazard evaluation in vulnerable areas. The information can be used to prioritize site visits and target on-site measurements.

4 Discussion

The available PSI dataset over Canton Wallis (Kanton Wallis, a) provides information covering an area wider than the Permos network and this deformation information could help in delimiting the ice-rich permafrost more efficiently. We discuss two specific examples where the PGIM could benefit from the PSI map.

The first case consists of area with PS showing significant displacements, i.e., greater than 10 mm/y, just outside the current mapped ice-rich permafrost (zone-2), see Fig. 7. These displacements could be a indication that permafrost zone-2 needs to be

https://doi.org/10.5194/egusphere-2023-2321
Preprint. Discussion started: 21 December 2023

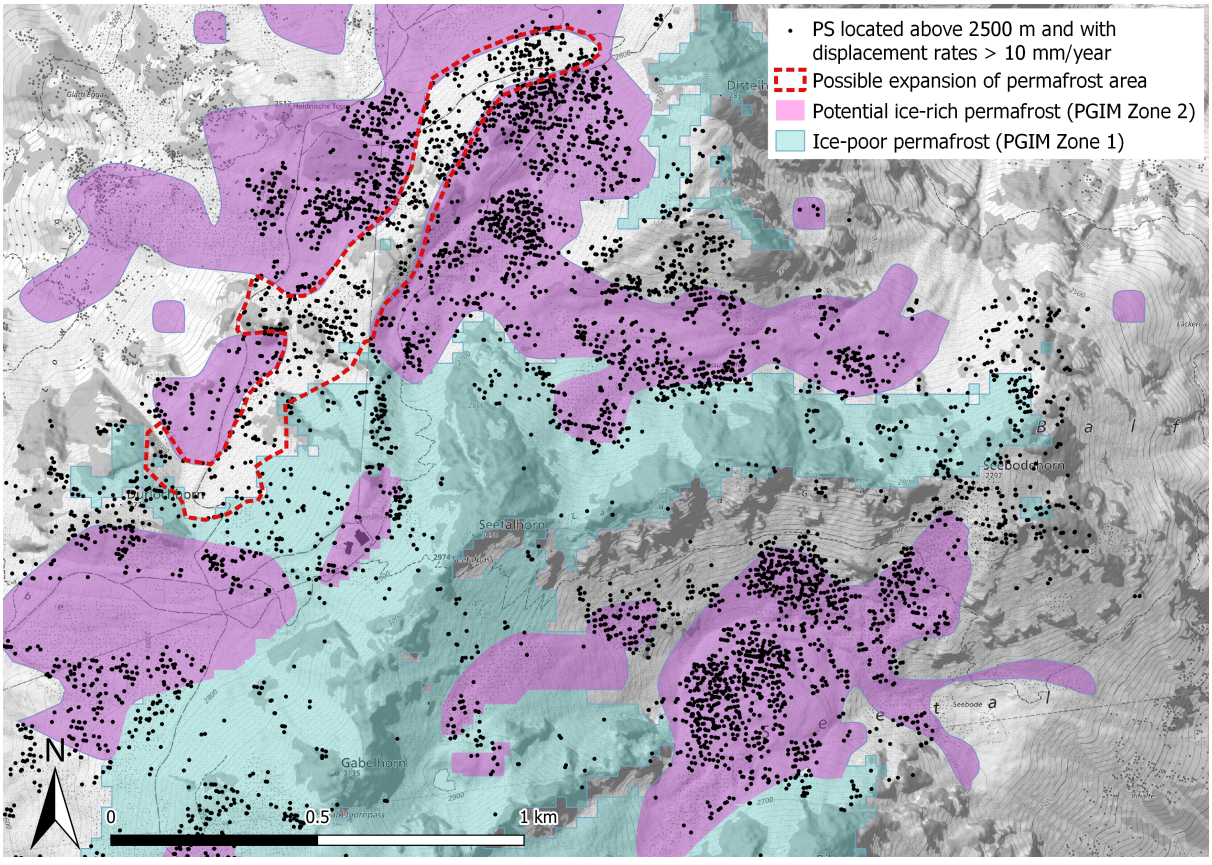

Figure 7. Permafrost zone-1 and zone-2 according to PGIM and PS with displacement rates greater than 10 mm/y, location near Stalden.

extended to that area. With this additional information, targeted field measurements campaigns can be set-up, in particular in areas that are critical in terms of risk for humans and infrastructure.

The second case consists of areas that are mapped as ice-rich permafrost in the PGIM but show displacements between -2 and $+2$ mm/year according to the PSI map, which indicates no significant (or very limited) movement. Fig. 8 presents an example of such a location.

The patches with these small displacements are mapped as ice-rich permafrost but may in reality contain no ice-rich permafrost. Not all mapped ice-rich permafrost zones necessarily contain PSI with large deformations. PS showing little motion can be related to the fact that (1) this area is not actually ice-rich, (2) the motion is dominantly orthogonal to the LoS, (3) the ice is not melting as rapidly as in other ice-rich areas and therefore movements are very small, or (4) the extent of frozen body is no longer sufficient to trigger internal deformations in the ice and thus creep movements (Krainer, 2015; Jones et al., 2019), and the rock glacier has come to a standstill. Also not all areas showing larger deformations in the PSI map are necessarily ice-rich permafrost zones. A thorough knowledge of geomorphology is required to distinguish between permafrost related deformations and other processes (RGIK, 2023).

https://doi.org/10.5194/egusphere-2023-2321
Preprint. Discussion started: 21 December 2023

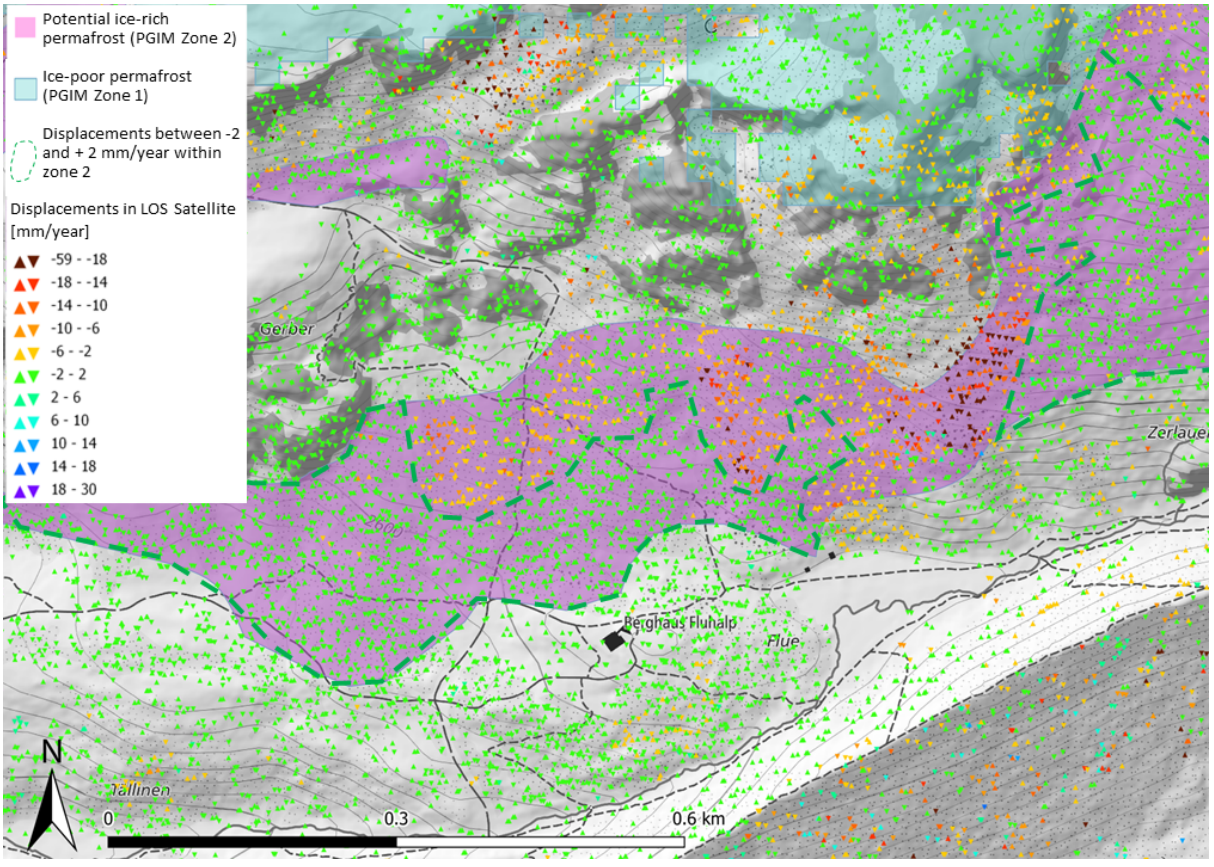

Figure 8. Permafrost zone-2 according to PGIM and PS with displacement rates, location Fluhalp Berghaus Zermatt.

Thus, although the available PSI map of Canton Wallis cannot be generically used to update the PGIM it can be used at specific locations for delimiting the ice-rich permafrost (zone-2 in the PGIM) more accurately and add important information on the state of activity. This supports the findings of RGIK (2023), Strozzi et al. (2020) and Brencher et al. (2020), who demonstrated how targeted InSAR analyses can be used as an additional source of information to delimit and map rock glaciers more accurately.

Finally we emphasise the limitations InSAR. All displacements are projected onto the Line of Sight (LoS) of the satellite. To convert these LoS displacement into a downslope and a normal component, PS of an ascending and descending orbit at the same location are necessary (Brouwer and Hanssen, 2023a, b). The precision with which these components can be estimated is location dependent. Moreover, the presence of snow results in the loss of coherence. In this study snow images where removed resulting in a smaller number of useful images per year. Furthermore the phase aliasing limits and resolving the correct ambiguity level when converting the radar data to displacements can be a constraint (Manconi, 2021; Reinders et al., 2021; Barboux et al., 2015).

https://doi.org/10.5194/egusphere-2023-2321
Preprint. Discussion started: 21 December 2023

5 Conclusion and future outlook

In this study, the performance of PSI interferometry based on Sentinel-1 data in the Swiss Alps was assessed. First we evaluated the sensitivity to radar detection of entire Switzerland. A necessary but not sufficient condition for this objective is the geometric visibility of the terrain, given a particular slope distribution and given satellite orbital geometries. We found that 92% of the areas currently labeled as permafrost in the Swiss Alps according to the recently published permafrost map (PGIM) satisfy the geometric visibility criteria. Second, we used a publicly available PSI dataset over Canton Wallis (Kanton Wallis, a) and found that non-zero PSI-derived surface displacement rates appear to be correlated with zones currently labeled as permafrost. The mean ground movement estimated over ice-rich permafrost zones is two to three times greater compared to mean ground deformations of the no-permafrost zones. In contrast, the mean ground movement of the ice-poor permafrost zones is only 1.2–1.3 times greater than the no-permafrost zones. While these differences in the means are statistically significant, the width of the distribution does not allow for using observed local displacements for directly discriminating permafrost zones. Yet, as ice-rich permafrost zones are typically situated between ice-poor en no-permafrost zones, the detection of—or absence of—significant displacements in the boundary between ice-rich and ice-poor permafrost can help in updating the geometry of the boundary between them in alpine permafrost maps.

As the quality of conventional alpine permafrost maps is limited by the scarcity of representative observational data, regional Persistent Scatterer Interferometry (PSI) can be used to evaluate, validate, and potentially improve alpine permafrost maps. While advanced application-aligned PSI results will always be more optimal, we find that application-agnostic PSI results that are publicly available can be used for this purpose. The information can be used for identifying and prioritising site visits and in-situ monitoring activities. The advent of new SAR satellite missions with different viewing geometries and revisit times, combined with contextual InSAR analysis, will further increase this potential.

https://doi.org/10.5194/egusphere-2023-2321
Preprint. Discussion started: 21 December 2023

Declaration of competing interest

The authors declare that they have no known competing financial interests of personal relationships that could have appeared to influence the work reported in this paper.

Author contributions

KR wrote the paper, set up the research idea and performed the research. GV provided the GIS analyses and maps. LS prepared the Sentinel-1 data to produce the R-index. AM supervised the research and reviewed the article. RH reviewed the manuscript.

Code/Data availability

We used freely available data. For the calculation of the R-index we used Sentinel-1 data downloaded from the Copernicus Open Access Hub (The European Space Agency, a) and the ESA SNAP Sentinel-1 toolbox (The European Space Agency, b). For the permafrost assessments we used the Persistent Scatterer Interferometry (PSI) map of Canton Wallis (Kanton Wallis, a), the Permafrost and ground ice map of Switzerland (PGIM) (SLF) and data from the Permos network (PERMOS).

https://doi.org/10.5194/egusphere-2023-2321
Preprint. Discussion started: 21 December 2023

References

Abe, T., Iwahana, G., Efremov, P. V., Desyatkin, A. R., Kawamura, T., Fedorov, A., Zhegusov, Y., Yanagiya, K., and Tadono, T.: Surface displacement revealed by L-band InSAR analysis in the Mayya area, Central Yakutia, underlain by continuous permafrost, Earth, Planets and Space, 72, 1–16, 2020.

Auer, I., Böhm, R., Jurkovic, A., Lipa, W., Orlik, A., Potzmann, R., Schöner, W., Ungersböck, M., Matulla, C., Briffa, K., et al.: HISTALP—historical instrumental climatological surface time series of the Greater Alpine Region, International Journal of Climatology: A Journal of the Royal Meteorological Society, 27, 17–46, 2007.

Baral, P., Allen, S., Steiner, J. F., Gurung, T. R., and McDowell, G.: Climate change impacts and adaptation to permafrost change in High Mountain Asia: a comprehensive review, Environmental Research Letters, 2023.

Barboux, C., Delaloye, R., Lambiel, C., Strozzi, T., Collet, C., and Raetzo, H.: Surveying the activity of permafrost landforms in the Valais Alps with InSAR, Mattertal–ein Tal in Bewegung, edited by: Graf, C., Publikation zur Jahrestagung der Schweizerischen Geomorphologischen Gesellschaft, 29, 7–19, 2013.

Barboux, C., Strozzi, T., Delaloye, R., Wegmüller, U., and Collet, C.: Mapping slope movements in Alpine environments using TerraSAR-X interferometric methods, ISPRS journal of photogrammetry and remote sensing, 109, 178–192, 2015.

BGR: BodenBewegungsdienst Deutschland, https://bodenbewegungsdienst.bgr.de/mapapps/resources/apps/bbd/index.html?lang=de, last access 03-11-2022.

Brencher, G., Handwerger, A. L., and Munroe, J. S.: InSAR-based characterization of rock glacier movement in the Uinta Mountains, Utah, USA., Cryosphere Discussions, 2020.

Brouwer, W. S. and Hanssen, R. F.: A treatise on InSAR geometry and 3D displacement estimation, IEEE Transactions on Geoscience and Remote Sensing, in press, https://doi.org/https://doi.org/10.31223/X55D37, 2023a.

Brouwer, W. S. and Hanssen, R. F.: Estimating Three-Dimensional Displacement with InSAR: the Strapdown Approach, Journal of Geodesy, submitted, https://doi.org/https://doi.org/10.31223/X5XM34, 2023b.

Bundesamt für Umwelt: Hinweiskarte der potenziellen Permafrostverbreitung, https://www.bafu.admin.ch/bafu/de/home/themen/naturgefahren/fachinformationen/naturgefahrensituation-und-raumnutzung/gefahrengrundlagen/hinweiskarte-der-permafrostverbreitung-in-der-schweiz.html#:~:text=Die%20Hinweiskarte%20der%20potenziellen%20Permafrostverbreitung%20in%20der%20Schweiz%20dient%20einer,Bauwerken%20in%20Verbreitungsgebieten%20von%20Permafrost, last access 26-01-2022, 2005.

CH2018: CH2018 – Climate Scenarios for Switzerland, Technical Report, National Centre for Climate Services, Zurich, 271 pp, 2018.

Chang, L., Dollevoet, R. P., and Hanssen, R. F.: Monitoring line-infrastructure with multisensor SAR interferometry: products and performance assessment metrics, IEEE j. of selected topics in applied earth observations and remote sens., 11, 1593–1605, 2018.

Cohen, J.: Statistical Power Analysis for the Behavioral Sciences (2nd ed., Lawrence Erlbaum Associates, Hillsdale NJ, 1988.

Crosetto, M., Solari, L., Mróz, M., Balasis-Levinsen, J., Casagli, N., Frei, M., Oyen, A., Moldestad, D. A., Bateson, L., Guerrieri, L., et al.: The evolution of wide-area DInSAR: From regional and national services to the European Ground Motion Service, Remote Sensing, 12, 2043, 2020.

Daout, S., Doin, M.-P., Peltzer, G., Socquet, A., and Lasserre, C.: Large-scale InSAR monitoring of permafrost freeze-thaw cycles on the Tibetan Plateau, Geophysical Research Letters, 44, 901–909, 2017.

https://doi.org/10.5194/egusphere-2023-2321
Preprint. Discussion started: 21 December 2023

Del Soldato, M., Solari, L., Novellino, A., Monserrat, O., and Raspini, F.: A New Set of Tools for the Generation of InSAR Visibility Maps over Wide Areas, Geosciences, 11, https://doi.org/10.3390/geosciences11060229, 2021.

Delaloye, R., Lambiel, C., and Gärtner-Roer, I.: Overview of rock glacier kinematics research in the Swiss Alps, Geographica Helvetica, 65, 135–145, 2010.

EGMS: European Ground Motion Service, Copernicus Programm of the European Union, https://land.copernicus.eu/pan-european/european-ground-motion-service, last access 03-11-2022.

Etzelmüller, B., Guglielmin, M., Hauck, C., Hilbich, C., Hoelzle, M., Isaksen, K., Noetzli, J., Oliva, M., and Ramos, M.: Twenty years of European mountain permafrost dynamics—the PACE legacy, Environmental Research Letters, 15, 104 070, 2020.

Giardino, J. R., Regmi, N. R., and Vitek, J. D.: Rock Glaciers, pp. 943–948, Springer Netherlands, Dordrecht, https://doi.org/10.1007/978-90-481-2642-2_453, 2011.

Goodfellow, B. W. and Boelhouwers, J.: 7.31 Hillslope processes in cold environments: an illustration of high-latitude mountain and hillslope processes and forms, Treatise on Geomorphology, pp. 320–336, 2013.

Gruber, S. and Haeberli, W.: Permafrost in steep bedrock slopes and its temperature-related destabilization following climate change, Journal of Geophysical Research: Earth Surface, 112, 2007.

Hanssen, R. F.: Radar Interferometry: Data Interpretation and Error Analysis, Kluwer Academic Publishers, Dordrecht, https://doi.org/10.1007/0-306-47633-9, 2001.

Hock, R., Rasul, G., Adler, C., Cáceres, B., Gruber, S., Hirabayashi, Y., Jackson, M., Kääb, A., Kang, S., Kutuzov, S., et al.: High mountain areas, 2019.

IPCC: Global warming of 1.5° C: an IPCC special report on the impacts of global warming of 1.5° C above pre-industrial levels and related global greenhouse gas emission pathways, in the context of strengthening the global response to the threat of climate change, sustainable development, and efforts to eradicate poverty, Intergovernmental Panel on Climate Change, 2018.

Jones, D. B., Harrison, S., Anderson, K., and Whalley, W. B.: Rock glaciers and mountain hydrology: A review, Earth-Science Reviews, 193, 66–90, 2019.

Jones, N., Strozzi, T., Rabatel, A., Ducasse, E., and Mouginot, J.: Surface instability mapping in alpine paraglacial environments using Sentinel-1 DInSAR techniques, IEEE Journal of Selected Topics in Applied Earth Observations and Remote Sensing, pp. 1–22, https://doi.org/10.1109/JSTARS.2023.3287285, 2023.

Kanton Wallis: https://guardaval.apps.vs.ch/information, last access on 02-08-2023, a.

Kanton Wallis: Kanton Wallis, https://www.vs.ch/de/web/plateforme-eau/dangers-naturels, last access on 19-07-2023, b.

Kenner, R., Noetzli, J., Hoelzle, M., Raetzo, H., and Phillips, M.: Distinguishing ice-rich and ice-poor permafrost to map ground temperatures and ground ice occurrence in the Swiss Alps, The Cryosphere, 13, 1925–1941, 2019.

Krainer, K.: Kapitel 1| Blockgletscher: Einführung, Publikationen Alpine Forschungsstelle Obergurgl, 2015.

Krautblatter, M., Funk, D., and Günzel, F. K.: Why permafrost rocks become unstable: a rock–ice-mechanical model in time and space, Earth Surface Processes and Landforms, 38, 876–887, 2013.

Li, R., Li, Z., Han, J., Lu, P., Qiao, G., Meng, X., Hao, T., and Zhou, F.: Monitoring surface deformation of permafrost in Wudaoliang Region, Qinghai–Tibet Plateau with ENVISAT ASAR data, International Journal of Applied Earth Observation and Geoinformation, 104, 102 527, 2021.

Liu, L., Schaefer, K., Chen, A., Gusmeroli, A., Zebker, H., and Zhang, T.: Remote Sensing Measurements of Thermokarst Subsidence Using InSAR, Journal of Geophysical Research: Earth Surface, 120, n/a–n/a, https://doi.org/10.1002/2015JF003599, 2015.

https://doi.org/10.5194/egusphere-2023-2321
Preprint. Discussion started: 21 December 2023

Liu, S., Zhao, L., Wang, L., Zhou, H., Zou, D., Sun, Z., Xie, C., and Qiao, Y.: Intra-Annual Ground Surface Deformation Detected by Site Observation, Simulation and InSAR Monitoring in Permafrost Site of Xidatan, Qinghai-Tibet Plateau, Geophysical Research Letters, 49, e2021GL095 029, 2022.

Macchiarulo, V., Milillo, P., Blenkinsopp, C., Reale, C., and Giardina, G.: Multi-Temporal InSAR for transport infrastructure monitoring: Recent trends and challenges, in: Proceedings of the Institution of Civil Engineers-Bridge Engineering, pp. 1–26, Thomas Telford Ltd, 2022.

Magnin, F., Josnin, J.-Y., Ravanel, L., Pergaud, J., Pohl, B., and Deline, P.: Modelling rock wall permafrost degradation in the Mont Blanc massif from the LIA to the end of the 21st century, The Cryosphere, 11, 1813–1834, 2017.

Manconi, A.: How phase aliasing limits systematic space-borne DInSAR monitoring and failure forecast of alpine landslides, Engineering Geology, 287, 106 094, 2021.

Meteoschweiz: Meteoschweiz, https://www.meteoschweiz.admin.ch/, last access 19-04-2022.

NCG: Bodemdalingskaart, https://bodemdalingskaart.nl/en-us/, last access 03-11-2022.

NGU, NVE, and the Norwegian Space Agency: InSARNorway, https://insar.ngu.no/, last access 03-11-2022.

Noetzli, J. and Pellet, C. e.: PERMOS 2023. Swiss Permafrost Bulletin 2022, No.4, https://doi.org/10.13093/permos-bull-23, 2023.

Noetzli, J. and Phillips, M.: Mountain permafrost hydrology, Hydro-CH2018 Project, Bern: Federal Office for the Environment, 18, 2019.

Noetzli, J., Gruber, S., Kohl, T., Salzmann, N., and Haeberli, W.: Three-dimensional distribution and evolution of permafrost temperatures in idealized high-mountain topography, Journal of Geophysical Research: Earth Surface, 112, 2007.

Noetzli, J., Arenson, L. U., Bast, A., Beutel, J., Delaloye, R., Farinotti, D., Gruber, S., Gubler, H., Haeberli, W., Hasler, A., Hauck, C., Hiller, M., Hoelzle, M., Lambiel, C., Pellet, C., Springman, S. M., Vonder Muehll, D., and Phillips, M.: Best Practice for Measuring Permafrost Temperature in Boreholes Based on the Experience in the Swiss Alps, Frontiers in Earth Science, 9, https://doi.org/10.3389/feart.2021.607875, 2021.

Notti, D., Herrera, G., Bianchini, S., Meisina, C., García-Davalillo, J. C., and Zucca, F.: A methodology for improving landslide PSI data analysis, International Journal of Remote Sensing, 35, 2186–2214, 2014.

Patton, A. I., Rathburn, S. L., and Capps, D. M.: Landslide response to climate change in permafrost regions, Geomorphology, 340, 116–128, https://doi.org/https://doi.org/10.1016/j.geomorph.2019.04.029, 2019.

Penna, I., Magnin, F., Nicolet, P., Etzelmüller, B., Hermanns, R., Böhme, M., Kristensen, L., Nöel, F., Bredal, M., and Dehls, J.: Permafrost controls the displacement rates of large unstable rock-slopes in subarctic environments, Global and Planetary Change, p. 104017, 2022.

PERMOS: PERMOS DATABASE. Swiss Permafrost Monitoring Network Database, Fribourg and Davos, Switzerland, https://doi.org/10.13093/permos-2022-01, last access on 01-06-2023.

Ravanel, L., Magnin, F., and Deline, P.: Impacts of the 2003 and 2015 summer heatwaves on permafrost-affected rock-walls in the Mont Blanc massif, Science of the Total Environment, 609, 132–143, 2017.

Reinders, K. J., Hanssen, R. F., van Leijen, F. J., and Korff, M.: Augmented satellite InSAR for assessing short-term and long-term surface deformation due to shield tunnelling, Tunnelling and Underground Space Technology, 110, 103 745, 2021.

Reinders, K. J., Giardina, G., Zurfluh, F., Ryser, J., and Hanssen, R. F.: Proving compliance of satellite InSAR technology with geotechnical design codes, Transportation Geotechnics, 33, 100 722, 2022.

RGIK: Towards standard guidelines for inventorying rock glaciers: baseline concept (version 4.2.1), IPA Action Group Rock glacier inventories and kinematics (Ed.), pp. 1–13, 2021.

https://doi.org/10.5194/egusphere-2023-2321
Preprint. Discussion started: 21 December 2023

RGIK: InSAR-based kinematic attribute in rock glacier inventories (Practical InSAR Guidelines v.4.0), IPA Action Group Rock glacier inventories and kinematics (Ed.), pp. 1–31, 2023.

Rouyet, L., Lauknes, T. R., Christiansen, H. H., Strand, S. M., and Larsen, Y.: Seasonal dynamics of a permafrost landscape, Adventdalen, Svalbard, investigated by InSAR, Remote Sensing of Environment, 231, 111 236, https://doi.org/https://doi.org/10.1016/j.rse.2019.111236, 2019.

Sawilowsky, S. S.: New effect size rules of thumb, Journal of modern applied statistical methods, 8, 26, 2009.

SLF: Permafrost and ground ice map of the Swiss institute of snow and avalanche research, https://www.slf.ch/pgim, last access on 29-08-2023.

Strozzi, T., Caduff, R., Jones, N., Barboux, C., Delaloye, R., Bodin, X., Kääb, A., Mätzler, E., and Schrott, L.: Monitoring rock glacier kinematics with satellite synthetic aperture radar, Remote Sensing, 12, 559, 2020.

The European Space Agency: Copernicus Open Access Hub, https://scihub.copernicus.eu/, last access on 08-04-2022, a.

The European Space Agency: Sentinel Application Platform[SNAP], https://step.esa.int/main/toolboxes/snap/, last access on 08-04-2022, b.

Tukey, J. W.: Comparing individual means in the analysis of variance, Biometrics, pp. 99–114, 1949.

UNIFI: Tuscany Region WebGIS, DST-UNIFI University of Florence, Department of Earth Sciences and Centro di Competenza del Servizio Nazionale di Protezione Civile, https://geoportale.lamma.rete.toscana.it/difesa_suolo/#/viewer/openlayers/326, last access 03-11-2022.

van Natijne, A., Bogaard, T., van Leijen, F., Hanssen, R., and Lindenbergh, R.: World-wide InSAR sensitivity index for landslide deformation tracking, International Journal of Applied Earth Observation and Geoinformation, 111, 102 829, 2022a.

van Natijne, A. L., Bogaard, T. A., van Leijen, F. J., Hanssen, R. F., and Lindenbergh, R. C.: World-wide InSAR sensitivity index data set for landslide deformation tracking, https://doi.org/10.4121/14095777, online Data set, 2022b.

Wang, L., Zhao, L., Zhou, H., Liu, S., Hu, G., Li, Z., Wang, C., and Zhao, J.: Evidence of ground ice melting detected by InSAR and in situ monitoring over permafrost terrain on the Qinghai-Xizang (Tibet) Plateau, Permafrost and Periglacial Processes, 34, 52–67, 2023.

WSP and Skygeo: Saettningskartan, https://Saettningskartan.se/sv, last access 03-11-2022.